J. Fluid Mech. (1982), *vol.* 118, *pp.* 123–141
Printed in Great Britain

Convective response of a mass of water near 4 °C to a constant cooling rate applied on its boundaries

By L. ROBILLARD AND P. VASSEUR

École Polytechnique, Université de Montréal,
Department of Civil Engineering, Montreal, Canada

(Received 18 May 1981)

The transient natural convection of a mass of water confined within a closed cavity with wall temperature decreasing at a steady rate is considered. For situations where a linear density–temperature relationship can be assumed, a quasi-steady state following an initial transient may be reached, provided that the cooling rate applied to the wall is held constant long enough. Steady-state flow characteristics in the case of a specific geometry are functions of a single parameter, the Rayleigh number, in which a dimensionless temperature, based on the cooling rate, is used. For the particular case of water cooled through 4 °C, the temperature at which maximum density occurs, a linear variation of density with respect to temperature is no more acceptable. However, it can be assumed that a linear relationship between the water thermal-expansion coefficient and the temperature is valid in the neighbourhood of 4 °C. With such an assumption it is still possible to characterize the cooling process that follows the initial transient by a single parameter. Detailed numerical results are presented for the particular case of a square cavity. Existing experimental and numerical results for the case of a horizontal circular pipe are also discussed.

1. Introduction

Natural convection flows in cold water are strongly affected by the occurrence of a density extremum with temperature variation. Thus at a temperature $T = 3{\cdot}98$ °C, the density of water attains a maximum value, thereafter decreasing in a nonlinear manner as the temperature passes this critical value. It follows from this peculiar behaviour that the usual linear approximation of the temperature effect on density, used in conventional analysis, must be replaced by another more realistic density equation of state.

The convective motion of enclosed water, in the region of maximum density, has been studied in the past for several different geometries, boundary conditions and temperature gradients. For instance, Desai & Forbes (1975) and Watson (1972) have studied numerically the heat transfer and flow patterns in cold water in a rectangular enclosure with vertical boundaries maintained at different temperatures and with insulated horizontal boundaries. The transient behaviour of water contained in a rigid rectangular insulator and cooled from above to near freezing has been considered by Forbes & Cooper (1975). Vasseur & Robillard (1980) have studied the transient cooling of water, enclosed in a rectangular cavity with wall temperature maintained at 0 °C. Supercooling of water contained in an enclosure subjected to convective boundary conditions has been investigated by Cheng, Takeuchi & Gilpin (1978) for the case of

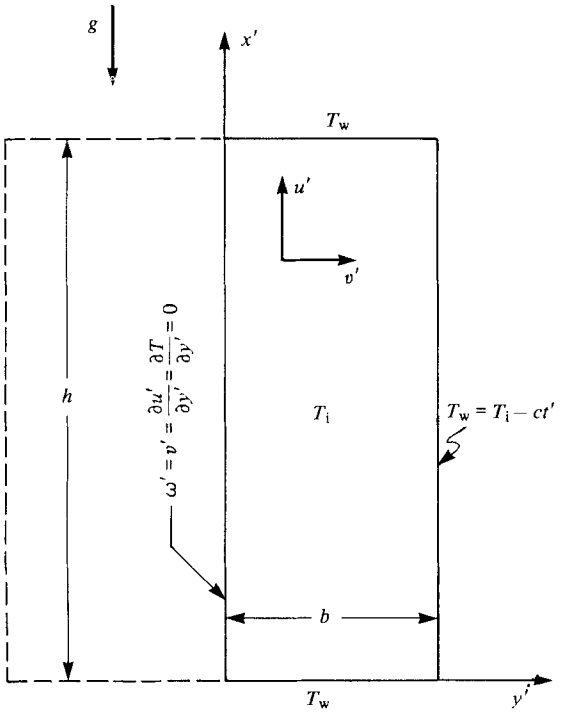

FIGURE 1. Co-ordinate system and boundary conditions.

a circular pipe and by Robillard & Vasseur (1981) for a rectangular cavity. It was found that the resulting flow motion is greatly influenced by the presence of a maximum-density effect. This latter slows down the initial circulation inside the cavity and subsequently reverses it. The resulting heat transfer is thus reduced in comparison to a standard situation without maximum-density effect.

Theoretical analysis of transient natural convection in enclosures with an initially uniform fluid temperature and a linear variation of wall temperature with time has received little attention in the literature. Prior studies of the subject have examined theoretically (Quack 1970; Takeuchi & Cheng 1976) and experimentally (Deaver & Ecker 1970) the transient natural convection in horizontal cylinders with constant cooling rate for temperature conditions such that there is no maximum-density effect. An experimental investigation of the cooling of water in a horizontal cylinder through the maximum-density point has been presented by Gilpin (1975). Results were found to be in agreement with Gilpin's quasi-steady-state boundary-layer model and a numerical study conducted by Cheng & Takeuchi (1976).

In this paper, the convection of a mass of water with boundaries cooled at a constant rate is considered through a dimensional analysis based on the assumption of a linear relationship between the thermal-expansion coefficient and the temperature. Cooling of the cavity is maintained long enough for the water temperature to encompass the 3·98 °C point. Exhaustive results for the specific case of a square cavity are obtained by a standard numerical method and conclusions of a general character are drawn. The particular thermal boundary conditions of the present problem, when applied to a rectangular cavity, introduce density gradients at the four boundaries. On the one

hand, driving forces are generated near the vertical walls in a way comparable to more-standard situations where the two vertical walls are maintained at different temperatures (e.g. Patterson & Imberger 1980). On the other hand an unstable layer is formed at one of the two horizontal walls, as when a cavity is heated from below (Linthorst, Schinkel & Hoogendoorn 1980).

2. Formulation of the problem

Consider the natural convective motion of a mass of water contained in the closed, rectangular two-dimensional cavity illustrated schematically in figure 1. The aspect ratio of the half-cavity is denoted by $E = h/b$. A rectangular Cartesian co-ordinate system is located in the centre of the base. Initially the water is motionless and at a uniform temperature T_1 higher than 3·98 °C. At time $t = 0$ a uniform temperature $T_w = T_1 - ct$, where c is a constant cooling rate, is imposed on the boundaries of the cavity. Cooling of the system is maintained long enough so that the water maximum temperature inside the cavity reaches a value below 3·98 °C.

The appropriate equations governing the resulting transient flow of fluid in this situation are

$$\frac{\partial u'}{\partial t'} + u'\frac{\partial u'}{\partial x'} + v'\frac{\partial u'}{\partial y'} = -\frac{1}{\rho_m}\frac{\partial p'}{\partial x'} - \frac{\rho}{\rho_m}g + \nu\nabla^2 u', \tag{1}$$

$$\frac{\partial v'}{\partial t'} + u'\frac{\partial v'}{\partial x'} + v'\frac{\partial v'}{\partial y'} = -\frac{1}{\rho_m}\frac{\partial p'}{\partial y'} + \nu\nabla^2 v', \tag{2}$$

$$\frac{\partial T}{\partial t'} + u'\frac{\partial T}{\partial x'} + v'\frac{\partial T}{\partial y'} = \frac{k}{\rho_m C_p}\nabla^2 T, \tag{3}$$

$$\frac{\partial u'}{\partial x'} + \frac{\partial v'}{\partial y'} = 0. \tag{4}$$

Here, u' and v' are the vertical and horizontal velocity components, T is the local temperature of fluid, p' the pressure, g the acceleration due to gravity, and ρ the density. ν, ρ_m, C_p, k and $\alpha = k/\rho_m C_p$ are respectively the kinematic viscosity, density, heat capacity, thermal conductivity, and thermal diffusivity, all referred to the temperature 3·98 °C corresponding to the maximum density (Veronis 1963), the present approach being valid in the neighbourhood of this point.

The initial and boundary conditions are:

$$u' = v' = 0, \quad T = T_1 \quad \text{everywhere} \quad \text{at} \quad t' = 0;$$

$$\text{for} \quad t' > 0 \quad \left\{ \begin{array}{l} u' = v' = 0, \quad T_w = T_1 - ct' \quad \text{on solid boundaries,} \\ \dfrac{\partial u'}{\partial y'} = v' = 0, \quad \dfrac{\partial T}{\partial y'} = 0 \quad \text{on the symmetry axis} \quad (y' = 0). \end{array} \right\} \tag{5}$$

Inherent in the derivation of (1) and (2) is the usual Oberbeck–Boussinesq approximation (Chandrashekar 1961; Gray & Giogini 1976). In addition, the compression and viscous-dissipation terms are neglected and all fluid properties are assumed constant except for density in the buoyancy term (Booker 1976). Each of these assumptions introduces certain small inaccuracies and the reference cited gives conditions under which these inaccuracies become significant. For the present study none is of major importance.

According to Moore & Weiss (1973), a parabolic-type relationship of the form

$$\frac{\rho-\rho_{\mathrm{m}}}{\rho_{\mathrm{m}}} = -\lambda(T-3{\cdot}98\ ^{\circ}\mathrm{C})^2 \tag{6}$$

with $\lambda = 8\times10^{-6}\ ^{\circ}\mathrm{C}^{-2}$ may be used within 4 % over the range 0–8 °C. The thermal-expansion coefficient becomes

$$\beta = -\frac{1}{\rho_{\mathrm{m}}}\frac{\partial\rho}{\partial T} = 2\lambda(T-3{\cdot}98\ ^{\circ}\mathrm{C}). \tag{7}$$

Defining the following dimensionless parameters:

$$\left.\begin{aligned} x &= \frac{x'}{b}, \quad y = \frac{y'}{b}, \quad u = \frac{u'b}{\alpha}, \quad v = \frac{v'b}{\alpha}, \\ t &= \frac{t'\alpha}{b^2}, \quad \theta = \frac{T-T_{\mathrm{w}}}{\Delta T}, \quad \Delta T = \frac{cb^2}{\alpha}; \end{aligned}\right\} \tag{8}$$

introducing a dimensionless stream function ψ and a dimensionless vorticity ω such that

$$u = \frac{\partial\psi}{\partial y}, \quad v = -\frac{\partial\psi}{\partial x}, \quad \omega = \frac{\partial v}{\partial x}-\frac{\partial u}{\partial y}; \tag{9}$$

and using (5)–(7), one can reduce (1)–(4) to the following non-dimensional forms:

$$\frac{1}{Pr}\left(\frac{\partial\omega}{\partial t}+\frac{\partial u\omega}{\partial x}+\frac{\partial v\omega}{\partial y}\right) = R\frac{\partial\theta}{\partial y}+R'\frac{\frac{1}{2}\partial\theta^2}{\partial y}+\nabla^2\omega, \tag{10}$$

$$\nabla^2\psi = -\omega, \tag{11}$$

$$\frac{\partial\theta}{\partial t}+\frac{\partial u\theta}{\partial x}+\frac{\partial v\theta}{\partial y} = \nabla^2\theta+1, \tag{12}$$

with initial and boundary conditions:

$$\text{at} \quad t=0 \quad u=v=\omega=\psi=\theta=0 \quad \text{everywhere};$$

$$\text{for} \quad t>0 \quad \left\{\begin{aligned} &u=v=\psi=\theta=0 \quad \text{at} \quad x=0,E, \quad y=1, \\ &\frac{\partial u}{\partial y}=v=\psi=\frac{\partial\theta}{\partial y}=\omega=0 \quad \text{at} \quad y=0. \end{aligned}\right\} \tag{13}$$

There are no boundary conditions for the vorticity, but indirectly

$$\left.\begin{aligned} \omega &= -\frac{\partial^2\psi}{\partial x^2} \quad \text{at} \quad x=0,E; \\ \omega &= -\frac{\partial^2\psi}{\partial y^2} \quad \text{at} \quad y=1. \end{aligned}\right\} \tag{14}$$

For the specific case of a square cavity containing water, $E=2$ and the Prandtl number $Pr=\nu/\alpha=11{\cdot}5$ corresponds to 3·98 °C. The value of unity ($b^2c\Delta T/\alpha=1$)

appearing on the right-hand side of the energy equation (12) can be regarded as a uniform-heat-source term. As a matter of fact, for situations where ρ is linearly related to T, the present problem is known to be equivalent to transient natural convection heat transfer between a fluid with uniform internal heat sources of strength per unit time and volume $\rho c C_p$ and a cavity with constant wall temperature.

The parameter R appearing in (10) is a time-dependent Rayleigh number defined as

$$R = \frac{gb^3}{\alpha\nu}\beta_w \Delta T, \tag{15}$$

where β_w is the thermal-expansion coefficient based on T_w, the temperature at the wall at a given time t. Since $\beta_w = \beta_1 - 2\lambda\Delta T t$ in the case of a parabolic relationship between ρ and T, (15) becomes

$$R = R_1 - R't, \tag{16}$$

where R_1 is an initial Rayleigh number based on temperature T_1. R' is a parameter called the nonlinear Rayleigh number. It corresponds to the rate of decrease of R, and is defined as

$$R' = \frac{gb^3}{\alpha\nu} 2\lambda\Delta T^2 = -\frac{\partial R}{\partial t}. \tag{17}$$

According to (10), nonlinear effects between density and temperature are expected to be small at a given time t if the condition

$$\frac{R'\theta}{|R|} \ll 1 \quad \text{or} \quad \frac{T - T_w}{|T_w - 3{\cdot}98\ ^\circ\text{C}|} \ll 1 \tag{18}$$

is satisfied.

In the numerical results, the dimensionless heat transfers across the top, lateral and bottom boundaries, denoted by ϕ_T, ϕ_L and ϕ_B respectively, are of interest. ϕ_T is defined as

$$\phi_T = \frac{q_T b}{k\Delta T} = \int_0^1 \left(-\frac{\partial\theta}{\partial x}\right)_{x=E} dy, \tag{19}$$

where ϕ_T is the heat flux per unit area averaged over the top boundary. ϕ_T is equivalent to a Nusselt number in which the characteristic temperature difference is based on the cooling rate c. Similar expressions may be obtained for lateral and bottom boundaries. Furthermore, it may be shown that the dimensionless heat transfer averaged over all boundaries corresponds to the following expression:

$$\phi_{av} = \frac{1}{2+E}(\phi_T + \phi_B + E\phi_L) = \frac{E}{2+E}\left(1 - \frac{\partial\bar{\theta}}{\partial t}\right), \tag{20}$$

where $\bar{\theta}$ is the dimensionless temperature averaged over the cavity according to the following equation:

$$\bar{\theta} = \frac{1}{E}\int_0^E \int_0^1 \theta\, dy\, dx. \tag{21}$$

$\bar{\theta}$ is a measure of the heat energy, in excess of the wall temperature, within the cavity.

3. Numerical approach

In this study a two-dimensional alternating direction (ADI) procedure is employed to solve the coupled transport and energy equations (10) and (12), which are quasi-linear, second-order partial differential equations of the parabolic type. The computational method involved differs slightly from that used by Mallison & de Vahl Davis (1973). The first and second derivatives are approximated by central differences and the time derivatives by a first-order forward difference. The finite-difference form of the equations are written in conservative form for the advective terms in order to preserve the conservative property (Roache 1976).

The elliptic equation (11) for the stream function, is solved by the method of successive over-relaxation (SOR). For the present problem it was found that a relaxation factor of 1·8 was an optimum value. The iterative procedure was repeated until the ratio of the maximum change in stream function occurring in the field as a result of one approximation to the maximum value of the stream function was smaller than 5×10^{-4}. In most of the calculations presented in this paper it was observed that the number of iterations required decreases rapidly from 30 immediately after the start of the cooling to 1–2 for most other time steps. It was also found that the number of iterations reaches as high as 20 when the maximum-density effect appears.

The specification of computational boundary conditions greatly affects the accuracy of the solution of the vorticity equation. Thus to be consistent with the accuracy of the scheme utilized in this study the wall vorticity was specified by a formulation similar to that developed by Woods (1954). Furthermore, it should be noted that, in conjunction with Woods' form, a consistent formulation of the velocity field for the grid points nearest the wall requires the use of a three-point special form obtained by a cubic equation. The velocity components computed in this way extrapolate smoothly to the wall.

The determination of an appropriate mesh size is related to the complex questions of accuracy and stability. Patterson & Imberger (1980), in their numerical treatment of the square cavity, use a time–length-scale approach to estimate the limits of time-step and mesh size for accurate spatial and temporal representation of the solution. They conclude that maintaining two mesh points inside the boundary layer at each vertical level requires an excessive number of points when R reaches 10^6. For the present study, a maximum mesh size of 30×15 for the half-cavity was found to be an acceptable compromise between the desired accuracy of the solution and the required computation time. It was also verified that the vortex formation was not influenced by the sweep direction in the SOR solution as it does for instance in a bottom-heated cavity. Typical values of the dimensionless time step were 0·0002, 0·0005 and 0·001.

A check of the conservative properties of the algorithm was made at regular intervals during the computation by comparing the heat transfer ϕ_{av} with the rate of change of $\bar{\theta}$ according to (20). Simpson's rule was used for numerical integration and a three-point finite-difference approximation for $\partial\bar{\theta}/\partial t$. The agreement between the results obtained by the two alternative relations given in (20) was found to be within 1–2 %.

To expedite plotting of the results, an auxiliary computer program was written to locate points lying on specified isotherms and streamlines by linear interpolation of the computed values at the grid points. As mentioned earlier, the problem under

consideration is symmetrical, and it was found advantageous to reproduce the flow and temperature fields at a given time on a single graph with the streamlines on the right half of the cavity and the isotherms on the left half.

4. Results and discussion

Equation (16) indicates that, when R' is set equal to zero, the resulting Rayleigh number R characterizing the present problem remains constant throughout the cooling process. This situation corresponds to the standard hypothesis of a linear relationship between density and temperature. However, if R' is given a finite value larger than zero, R decreases linearly with time. The resulting situation then corresponds to the cooling of a fluid having a parabolic relationship between its density and temperature, such as water at a temperature in the neighbourhood of 3·98 °C. Both situations will be discussed in the following sections.

4.1. *Results with R constant*

The cooling with constant R of a mass of fluid contained in a horizontal circular pipe has been studied theoretically by Quack (1970) and Takeuchi & Cheng (1976) and experimentally by Deaver & Ecker (1970). It was found that, although the cooling process is a transient one, a quasi-steady state develops if the cooling rate is held constant long enough. This quasi-steady state, as described by Takeuchi & Cheng, is characterized by temperature differences between interior points and boundary that remain constant with time. Figure 2(*a*) gives $\bar{\theta}$, the dimensionless temperature averaged over the cavity, as a function of the cooling time t, for $R = 5 \times 10^4$ and 3×10^5. The pure conduction case is reproduced for the purpose of comparison. For those three cases, at time $t = 0$, the fluid is motionless and at uniform temperature T_1. At the early stages of the cooling process, temperature gradients are set up near the walls. If motion is excluded, as it is the case for $|R| \to 0$, a pure-conduction quasi-steady state is reached for which $\bar{\theta} = 0{\cdot}14$. If motion is allowed, by setting R different from zero, driving forces introduced by density differences near the side walls generate convective flow, which takes the form of two counter-rotating vortices, with fluid moving downward near the side walls for $R > 0$. With time elapsing, a quasi-steady state is reached for which $\bar{\theta}$ becomes independent of time and $\phi_{\mathrm{av}} = 0{\cdot}5$, according to (20), in the case of a square cavity ($E = 2$). At the quasi-steady state, the value of $0{\cdot}14 - \bar{\theta}$ is a measure of the convective motion inside the cavity, this difference increasing with increasing R. Thus R represents a potential of convective motion, this latter being attained at steady state. The quasi-steady-state flow and temperature fields corresponding to $R = 5 \times 10^4$ are represented in figure 2(*b*) on the right and left half of the cavity respectively, the symmetry condition prevailing throughout the computation. The specific configuration of the isotherms on the left half indicates that the top heat transfer ϕ_{T} is larger than the bottom heat transfer ϕ_{B}.

Figure 2(*c*) corresponds to $R = 3 \times 10^5$, and implies a relatively high convective motion for which a second mode of convection, consisting of two additional rolls near the top boundary, is established inside the cavity. A comparable secondary motion has been reported by Tarunin (1968) for the case of a square cavity with wall temperature suddenly increased. Such a flow behaviour results essentially from the

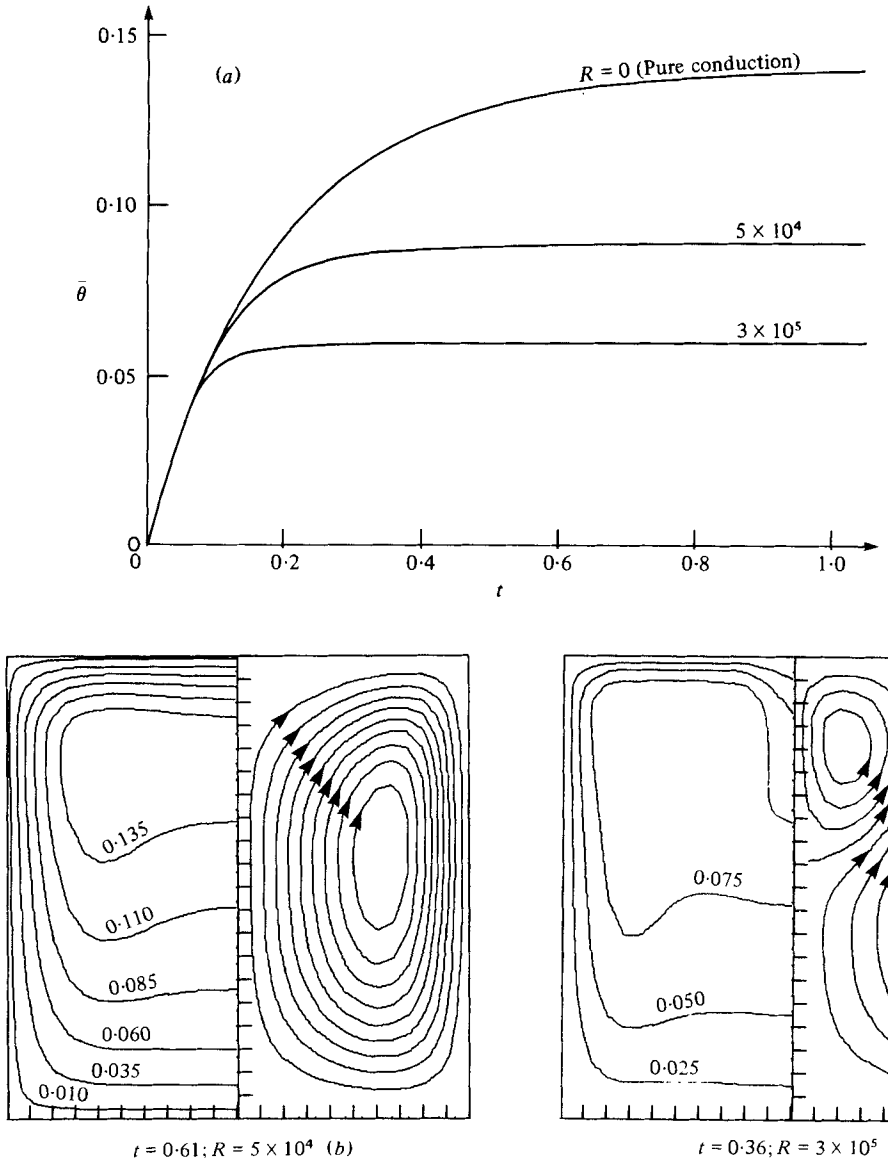

FIGURE 2. (*a*) Initial transients and (*b*, *c*) quasi-steady-state flow and temperature fields for R maintained constant with time.

interaction between the zone of instability located near the top boundary and the flow field induced by the side wall.

Quasi-steady-state results giving $\bar{\theta}$ as a function of R correspond to the heavy line of figure 3(*a*). This line may be obtained point by point by solving numerically the basic equations with $R' = 0$ far enough in time to obtain the quasi-steady state, the procedure being repeated for different R. Other steady-state characteristics are given by heavy lines of figures 3(*b*, *c*). The discontinuity observed on some of those lines is located at $R = \pm 8 \times 10^4$, and separates the first and second mode of convection already mentioned.

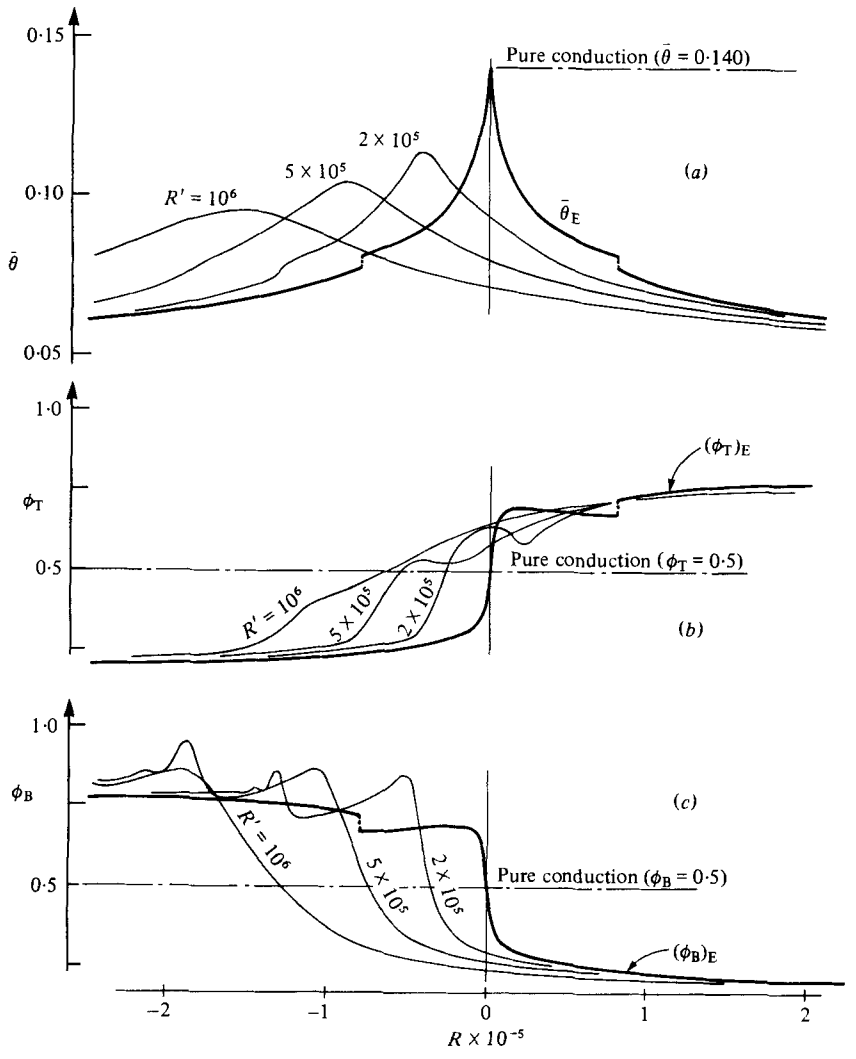

FIGURE 3. Quasi-steady-state or equilibrium curves (heavy lines) and nonlinear transients (light lines) in the case of dimensionless temperature averaged over the cavity (*a*), and dimensionless heat transfers across the top (*b*) and bottom (*c*) boundaries.

Results on figure 3 are shown with R on an arithmetic scale with negative range. The negative range corresponds to negative β_w in (15), i.e. to a situation for which density is decreasing with decreasing temperature, as it occurs for water below 3·98 °C. The flow and temperature fields at negative R are the mirror images of those at corresponding positive R. $(\phi_T)_E$ behaves as $(\phi_B)_E$ and vice versa. Such a behaviour can be noticed on figures 3(*b*, *c*). At $R = 0$, the heavy line $\bar{\theta}_E$ of figure 3(*a*) attains a maximum value of 0·14 with a sharp peak, whereas $(\phi_T)_E$ and $(\phi_B)_E$ of figures 3(*b*, *c*) take the value 0·5 with maximum slope. Thus extrema for $\bar{\theta}$ and the derivatives of ϕ_T and ϕ_B are seen to occur at $R = 0$.

Quasi-steady-state characteristics are also given on figure 4 with a logarithmic scale for R in order to cover the wide range involved in the numerical solution. Positive and negative ranges of R are superposed. As a consequence, figure 4(*c*) shows two heavy

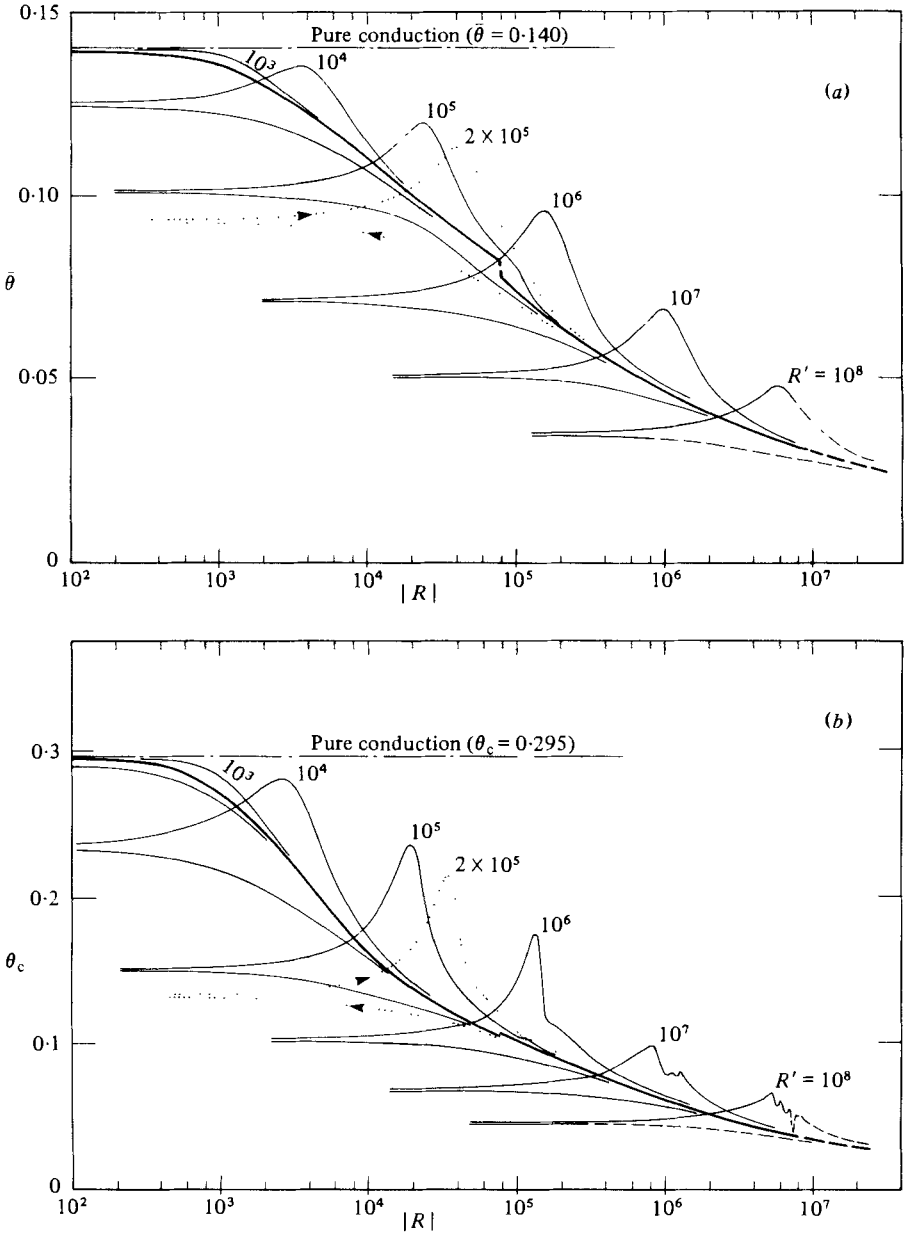

FIGURE 4. (*a*, *b*) for legend see opposite page.

lines, with the top one corresponding to positive R and the bottom one to negative R. The converse is true for figure 4(*d*).

4.2. *Results with R decreasing linearly with time*

When R decreases with time at a constant rate R', the initial transient is followed by a nonlinear transient, as illustrated in figure 5. In this figure, the time scale of figure 2(*a*) is replaced by a Rayleigh scale, which corresponds also to a temperature scale with 3·98 °C at $R = 0$. The three dashed lines are initial transients, with the same

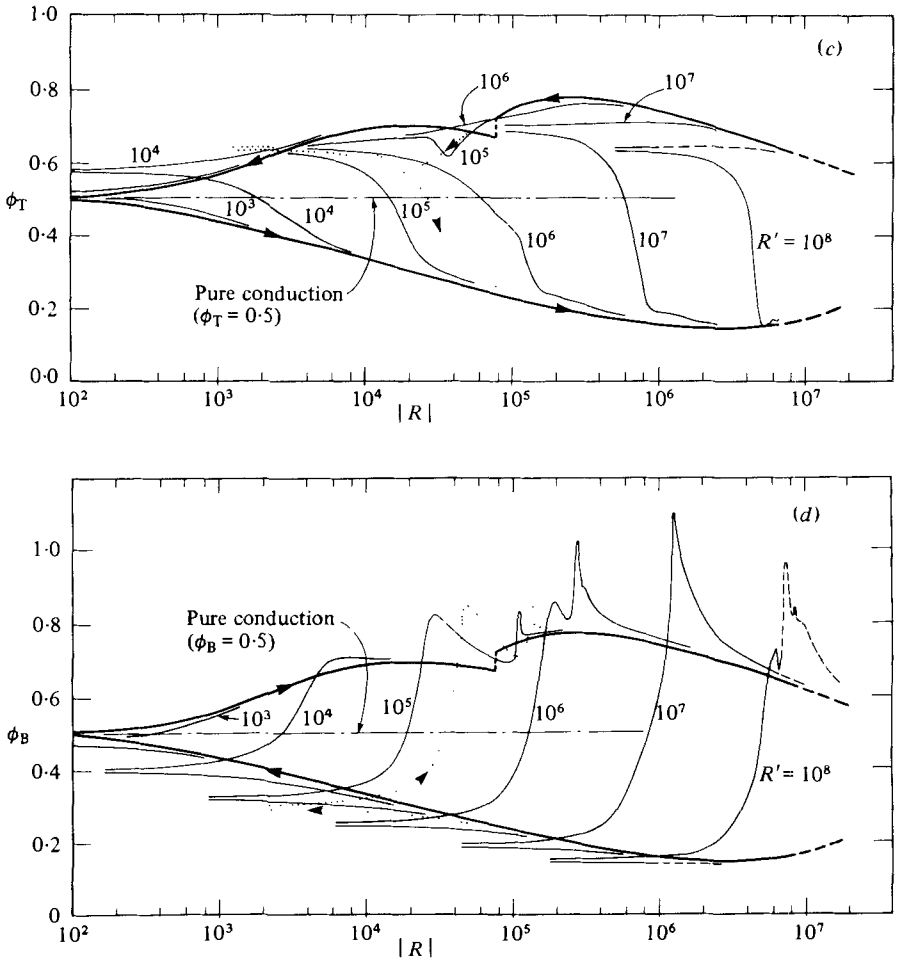

FIGURE 4. Dimensionless temperature (*a*) averaged over the cavity, (*b*) at the centre of the cavity; and heat transfer at (*c*) the top boundary, (*d*) the bottom boundary; plotted as functions of R. Heavy lines represent the quasi-steady-state (or equilibrium) curve, light and dotted lines the nonlinear transients.

$R' = 2 \times 10^5$ but different R_1. Those lines tend asymptotically to a single curve represented by a continuous line on figure 5. This curve is a nonlinear transient determined uniquely by the single parameter R'. Nonlinear transients exist for other physical quantities such as θ_c, heat transfers at boundaries or stream functions. Once relieved of the initial transients, they form all together the essential features of the cooling through a maximum density.

It is possible to obtain the nonlinear transients to their full extent by initiating the cooling process at a value R_1 such that nonlinear effects are absent, inequality (18) being satisfied for all interior points, and by providing enough computer time to reach negative R such that (18) is again satisfied. Nonlinear transients of figures 3 and 4 have been obtained through that approach. Among them are the nonlinear transients corresponding to $R' = 2 \times 10^5$ of figures 5 and 6. On figure 4, these latter are represented by dotted lines. The direction of the cooling process is indicated by arrows on figure 4. The heavy lines of figures 3 and 4 have already been described to

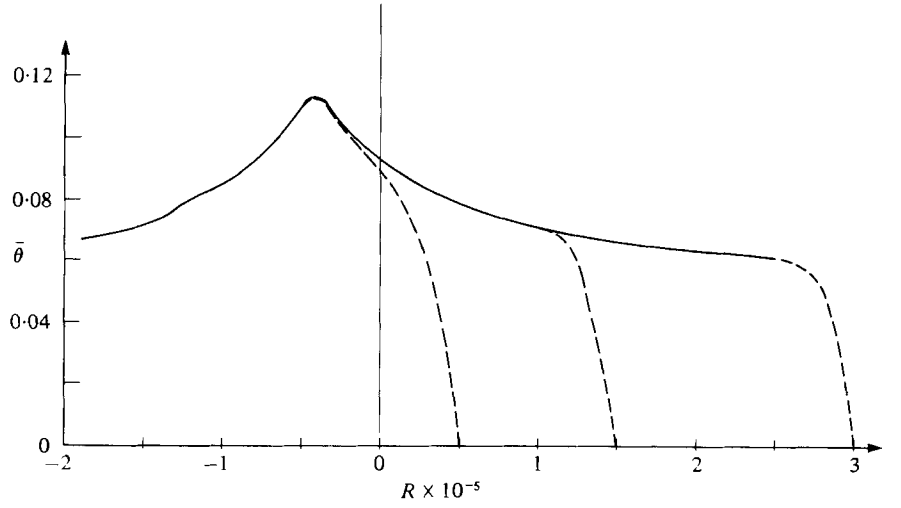

FIGURE 5. Initial (– – –) and nonlinear (——) transients for R decreasing linearly with time at a rate $R' = 2 \times 10^5$.

be quasi-steady states for cases where ρ varies linearly with T. Here they correspond to equilibrium states to which the fluid system tends, with a lag proportional to the rate of change of R. Nonlinear transients tend to join asymptotically the quasi-steady state or equilibrium curves when $R'\theta/R$ becomes negligibly small. It is observed on figure 3, that when R has decreased sufficiently, $\bar{\theta}$, ϕ_T and ϕ_B will depart from the equilibrium curves $\bar{\theta}_E$, $(\phi_T)_E$ and $(\phi_B)_E$ respectively, this departure occurring earlier for higher R'.

4.3. *The inversion process*

It may be observed on figure 3(*a*) that the peak corresponding to a given R' shows a more-or-less pronounced lag with respect to $R = 0$, the position along the abscissa where the peak of the equilibrium curve $\bar{\theta}_E$ is located. It is also observed that the peak value is smaller for larger R'. The pure conduction value of 0·14 for the equilibrium curve is due to the fact that, for $R' \to 0$, there is no more convective heat transfer at $R = 0$. However, for finite R', convective motion is transported toward negative R, and thus convective motion resulting from positive R is still present when negative-R effects are acting to reverse the flow field. As a matter of fact, once R has become negative, temperature differences introduced near the boundaries start generating density gradients of opposite sign. An inversion process is thus initiated inside the cavity at the end of which the flow and temperature fields tend to become the mirror image of the ones at corresponding positive R. The higher is R', the more intense is the convective motion inside the cavity during the inversion process. This fact explains why the peak characterizing the nonlinear transient decreases with increasing R'. With progression of the cooling process beyond the peak value for $\bar{\theta}$, i.e. with R becoming more negative, the density differences introduced near the boundaries become more pronounced. The new counter-rotating motion set up inside the cavity is reinforced, and convective heat transfer is enhanced. As a consequence, $\bar{\theta}$ begins to decrease. Condition (18) is more and more nearly satisfied and $\bar{\theta}$ tends asymptotically

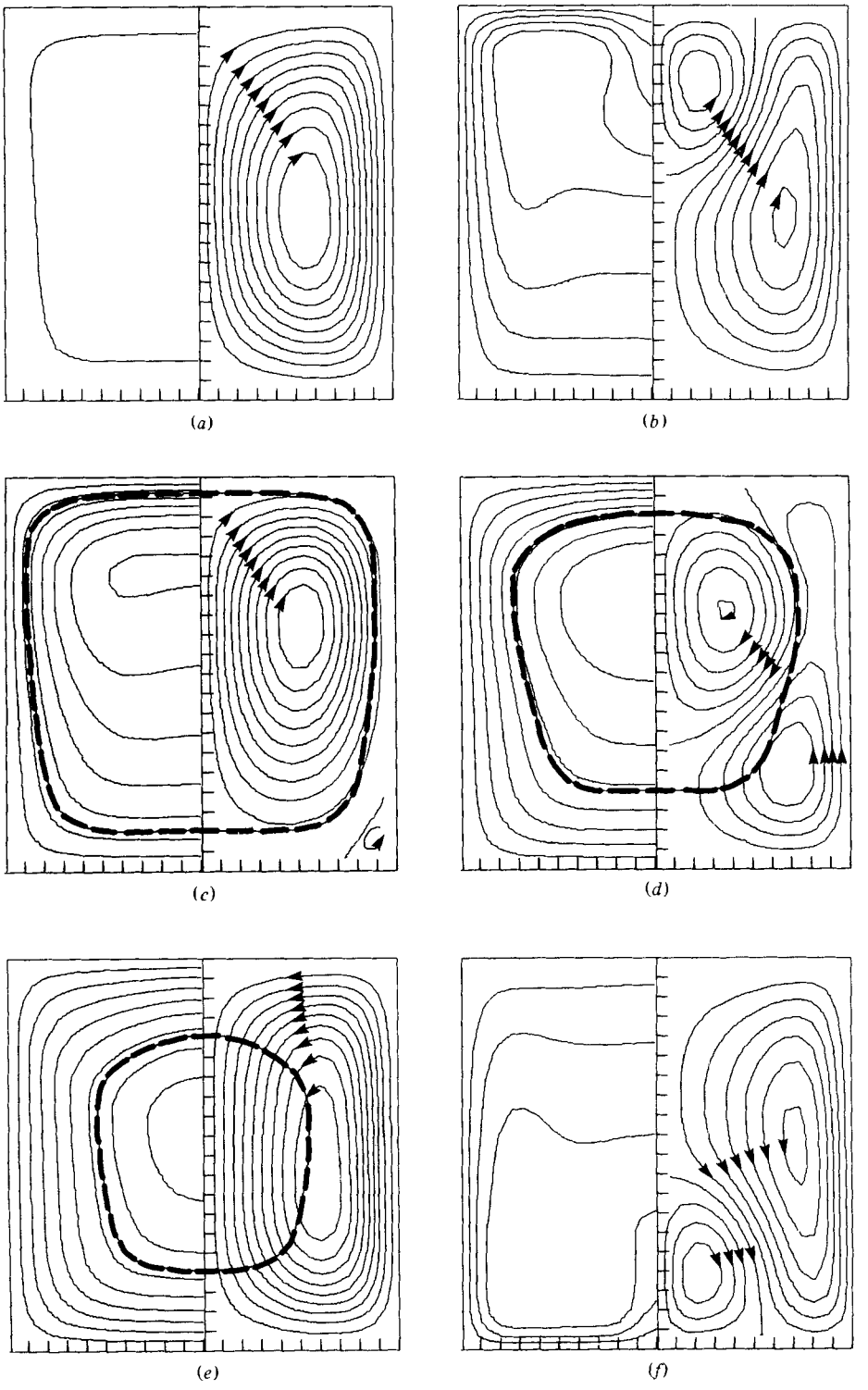

FIGURE 6. Transient streamlines and isotherm field with $\Delta\theta = 0{\cdot}025$, for $R' = 2 \times 10^5$ and $R_1 = 1{\cdot}47 \times 10^5$ (the dashed line, where it appears, represents the 3·98 °C isotherm). (*a*) $R = 1{\cdot}4 \times 10^5$; (*b*) $1{\cdot}01 \times 10^5$; (*c*) $-1{\cdot}24 \times 10^4$; (*d*) $-2{\cdot}45 \times 10^4$; (*e*) $-3{\cdot}25 \times 10^4$; (*f*) $-3{\cdot}0 \times 10^5$.

to the equilibrium curve. Nonlinear transients are therefore connected to the equilibrium curve in both positive and negative directions and this observation is true for the other physical quantities such as θ_c or heat transfers at boundaries.

The sequence of events taking place during the inversion process may be observed on the set of figures 6 (*a–f*), where flow and temperature fields corresponding to a moderate R' are illustrated. Figure 6 (*a*), with $R = 1{\cdot}4 \times 10^5$ corresponds to the initial transient described in § 4.2, during which temperature differences are being set up inside the cavity. The value of R_i involved in the present case ($1{\cdot}47 \times 10^5$) is important enough for a second mode of convection to develop, and, consequently, two pairs of counter-rotating vortices are present inside the cavity (figure 6*b*) when the initial transient is over (see also figure 5). The initiation of the inversion process is depicted by figure 6 (*c*), in which the occurrence of a small vortex of opposite rotation near the bottom corner indicates the beginning of the flow reversal. With time elapsing, this vortex grows and displaces the original one (figure 6*d*). Eventually a situation is reached where the original circulation is completely reversed, as shown on figure 6 (*e*). The new motion gradually brings the relatively warm fluid of the core region near the bottom boundary. With progression of the cooling process, the reversed convective motion is enhanced. A second mode of convection appears, with a pair of additional vortices near the bottom boundary, as shown on figure 6 (*f*). It is also noticed on this last figure that the temperature field, like the flow field, has become opposite in character to the one existing at positive R (compare with figure 6 (*c*) and also with figure 2 (*c*)).

4.4. *Transportive property of R′ toward low temperatures*

The extremum in density at 3·98 °C gives rise to a very important change in flow behaviour within the laminar range of the cooling process. There are, however, other important changes such as the passage from one mode of convection to another along the R axis. As mentioned in § 4.1 the passage is abrupt in the case of the equilibrium curves with a finite jump separating the first and second modes at $R = \pm 8 \times 10^4$. For $R' > 0$, the passage from one mode to the other occurs later and is more gradual. For instance, it may be observed on figure 3 (*a*) that the jump occurring at $R = -0{\cdot}8 \times 10^5$ on the $\bar{\theta}_E$ curve is reported approximately at $R = -1{\cdot}3 \times 10^5$ and $-1{\cdot}8 \times 10^5$ on the nonlinear transients corresponding to $R' = 2 \times 10^5$ and 5×10^5 respectively. Similar effects concerning the passage from one mode to the other are observed for the heat-transfer curves of figures 3 (*b*, *c*). Thus, considering the lag created by R' on the flow reversal at 3·98 °C and the lag also created by R' on the passage from one mode to the other, it may be concluded that an important property of R' is to transport toward negative R the features of the convection that characterize the equilibrium state. Moreover, if R' is important enough, the second mode occurring at positive R will not disappear before the initiation of the inversion process at $R \simeq 0$ and will interact with it. The sequence of flow and temperature fields of figures 7 (*a–f*) illustrates a case where R' is important enough for the secondary motion to be present when the inversion process starts. All figures of this sequence, including the first one, describe the non-linear transient exclusively, no initial transient being involved. It can be noticed that figure 7 (*f*) is almost the mirror image of figure 7 (*a*).

If very large values of $|R|$ are involved, the cooling process may start in the range of turbulent convection above 3·98 °C and also end up in the turbulent range below

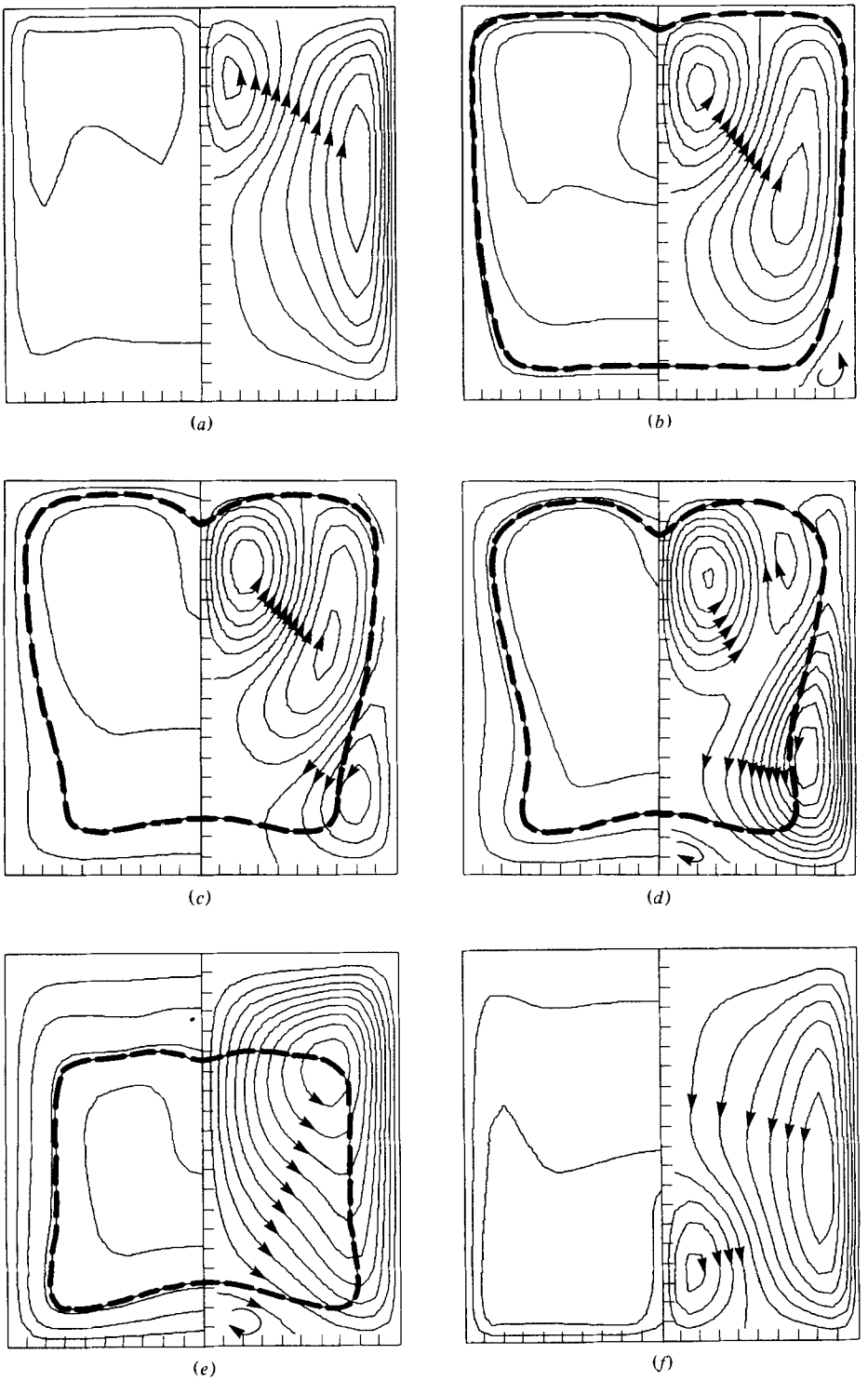

FIGURE 7. Transient streamlines and isotherm field with $\Delta\theta = 0{\cdot}025$, for $R' = 10^7$ (the dashed line, where it appears, represents the 3·98 °C isotherm). (*a*) $R = 3{\cdot}00 \times 10^5$; (*b*) $-3{\cdot}15 \times 10^5$; (*c*) $-5{\cdot}16 \times 10^5$; (*d*) $-6{\cdot}16 \times 10^5$; (*e*) $-8{\cdot}17 \times 10^5$; (*f*) $-3{\cdot}00 \times 10^6$.

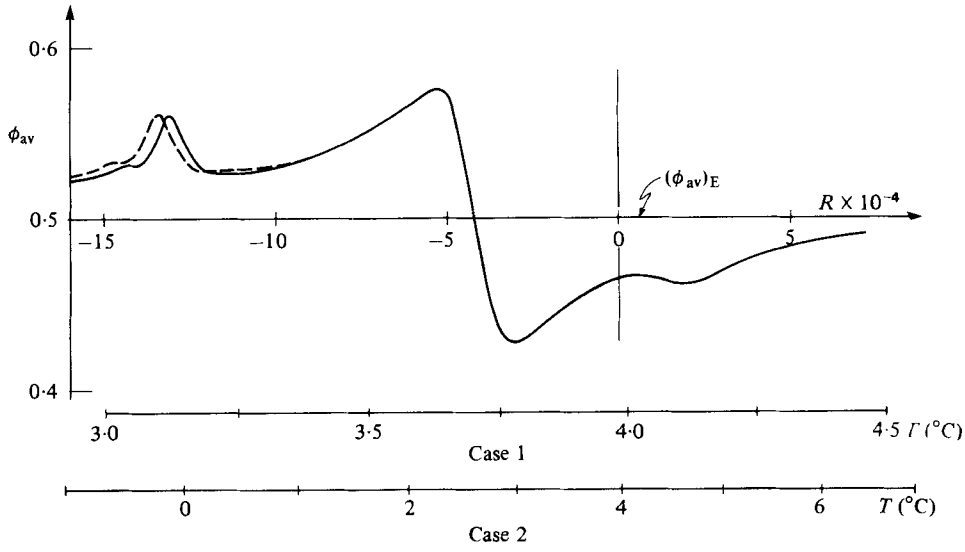

FIGURE 8. Discrepancies due to the nonlinearity in the relationship between β and T, affecting the heat transfer averaged over all boundaries, as defined in (20). $R' = 2 \times 10^5$ for both cases 1 (continuous line) and 2 (dashed line).

3·98 °C. Here also it might be expected that turbulent features will be carried toward lower R, thus reducing the laminar range. Large R' can be conceived for which turbulence is carried with enough strength to reach the inversion process and even to reach negative R where the reversed convection itself starts generating turbulence. If the initial transient occurs in the turbulent range, a laminar range for the nonlinear transient will follow provided that R' is not too large, i.e. provided that enough time is given for viscous forces to absorb the turbulent motion of the system. The present numerical computation is, of course, limited to the laminar range. When large R values ($R \sim 10^7$) are involved, oscillations develop in the numerical results, and parts of the curves corresponding to the occurrence of those oscillations are presented by dashed lines on figure 4.

4.5. *Effects of the nonlinearity in the relationship between β and T*

Each nonlinear transient of figures 3 and 4 describes adequately the behaviour of a mass of water cooled to a constant rate, provided that temperatures involved remain in the neighbourhood of 3·98 °C. Discrepancies will develop with increasing difference between T_w and 3·98 °C. In fact, owing to the nonlinearity between β and T, the rate of change of R is slightly increasing with decreasing temperature, c being maintained constant. This tendency is more-or-less pronounced at a particular R, depending on $|T_w - 3{\cdot}98\ °C|$. Strictly speaking, R' of (17) corresponds to the exact rate of change of R only when $T_w = 3{\cdot}98$ °C. Figure 8 illustrates the kind of discrepancy to be expected. The heat transfer ϕ_{av} is seen to vary in (20) according to $\partial\bar{\theta}/\partial t$. Two cases having the same R' are reproduced in figure 8. The computation of the two cases was done by using a fourth-order polynomial in the relationship between ρ and T. Case 1 covers a relatively narrow temperature range above and below 3·98 °C, as indicated by its temperature scale. Case 2 is represented by a dashed line where it differs significantly

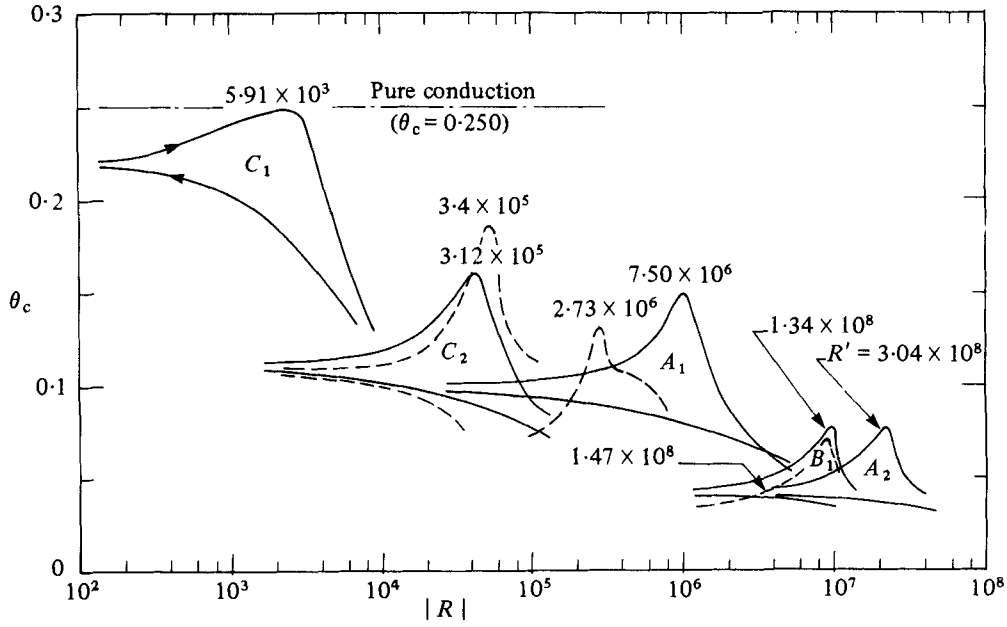

FIGURE 9. Dimensionless temperature at the centre of the cavity, as a function of R, in the case of a horizontal cylinder filled with water and cooled at a constant cooling rate (only non-linear transients are represented; no available data were found in existing literature from which an equilibrium curve could be derived). ——, experimental results (Gilpin 1975); – – –, numerical results (Cheng & Takeuchi 1976). Radii b and cooling rates c are as follows: A_1, b = 6·8 cm, c = 0·6 °C/h; A_2, 6·8 cm, 3·8 °C/h; B_1, 3·75 cm, 20·3 °C/h; C_1, 1·3 cm, 5·5 °C/h; C_2, 1·3 cm, 40·0 °C/h.

from case 1. The kind of discrepancy observed between the two cases provides an indication on the validity and the limits of the parabolic approach on which the present dimensional analysis is based.

4.6. *Comparison with existing experimental data*

In Gilpin's (1975) experiments on the cooling of a horizontal circular cylinder filled with water, the temperature at the centre was recorded as a function of time for various diameters and cooling rates. Those experimental results, transformed by the application of the present dimensional analysis, are shown on figure 9. It is observed that the trend of figure 4(*b*) is reproduced qualitatively. Numerical results obtained by Cheng & Takeuchi (1976) for the same type of problem have also been transformed and reproduced on figure 9. Those last curves are incomplete and not entirely relieved of the initial transients. Nevertheless their trend and ordering shows relatively good agreement with the previous ones.

5. Conclusions

The natural convection taking place in a mass of water near 3·98 °C with boundaries subjected to a constant cooling rate has been investigated through a dimensional analysis based on a parabolic relationship between density and temperature. Although most graphics presented in this article concern specific numerical method and geometry

(square cavity), general conclusions may be established with application to any geometry and to experimental as well as theoretical studies on the subject. In particular the following statements can be made.

(1) When density is linearly related to temperature, a quasi-steady-state regime may be reached from initial conditions for which the fluid is at rest and at uniform temperature. The transient solution is characterized by a developing regime during which motion is set up inside the cavity. At sufficiently large time, velocities, flow patterns and temperature differences between the fluid and the wall become constant with time, indicating that the quasi-steady state is reached.

(2) The presence of a maximum density, as is the case for water at 3·98 °C, implies a decrease followed by a reversal and finally an increase of the convective motion inside the cavity.

(3) When a maximum density is involved in the cooling process, nonlinear transients replace the quasi-steady-state results. Those nonlinear transients, relieved of the initial ones, are the essential features of the cooling process and are uniquely determined by a single parameter called the nonlinear Rayleigh number. The set of nonlinear transients obtained for different values of the nonlinear Rayleigh number forms an exhaustive solution for a given geometry.

(4) Quasi-steady-state results obtained when the density is linearly related to the temperature correspond to equilibrium curves to which nonlinear transients tend asymptotically when the difference $|T - 3{\cdot}98\ °C|$ is increased.

(5) An important effect of the nonlinear Rayleigh number is to transport toward low temperatures the features of convection characterizing the equilibrium curves. A lag is so created between the nonlinear transient and the corresponding equilibrium curve, the importance of this lag being directly related to the value of the nonlinear Rayleigh number.

This work was supported in part by the National Sciences and Engineering Research Council of Canada through grants A-4197 and A-9201 and jointly by the FCAC, Gouvernement du Québec, under grant number CRP 506-78.

REFERENCES

Booker, J. R. 1976 *J. Fluid Mech.* **76**, 741.

Chandrashekar, S. 1961 *Hydrodynamic and Hydromagnetic Stability.* Oxford University Press.

Cheng, K. C. & Takeuchi, M. 1976 *Trans. A.S.M.E.* C, *J. Heat Transfer* **98**, 581.

Cheng, K. C., Takeuchi, M. & Gilpin, R. 1978 *Numer. Heat Transfer* **1**, 101.

Deaver, F. K. & Eckert, E. R. G. 1970 In *Heat Transfer*, vol. 4, paper NC 1.1. Elsevier.

Desai, V. S. & Forbes, R. E. 1971 *Environ. Geophys. Heat Transfer* **4**, 41.

Forbes, R. E. & Cooper, J. W. 1975 *Trans. A.S.M.E.* C, *J. Heat Transfer* **97**, 47.

Gilpin, R. R. 1975 *Int. J. Heat Mass Transfer* **18**, 13.

Gray, D. D. & Giogini, A. 1976 *Int. J. Heat Mass Transfer* **19**, 545.

Linthorst, S. J. M., Schinkel, W. M. M. & Hoogendoorn, G. J. 1980 In *Proc. A.S.M.E. Nat. Heat Transfer Conf., Orlando*, HTD 8, 39.

Mallison, G. D. & de Vahl Davis, G. 1973 *J. Comp. Phys.* **12**, 435.

Moore, D. R. & Weiss, N. O. 1973 *J. Fluid Mech.* **61**, 553.

Patterson, J. & Imberger, J. 1980 *J. Fluid Mech.* **100**, 65.

Quack, H. 1970 *Wärme- und Stoffübertragung* **3**, 134.

ROACHE, P. 1976 *Computational Fluid Dynamics*. Hermose.
ROBILLARD, L. & VASSEUR, P. 1981 *Trans. A.S.M.E.* C, *J. Heat Transfer* **103**, 528.
TAKEUCHI, M. & CHENG, K. C. 1976 *Wärme- und Stoffübertragung* **9**, 215.
TARUNIN, E. L. 1968 *Izv. Akad. Nauk S.S.S.R. Mech. Zhid. i Gaza* **3**, 83.
VASSEUR, P. & ROBILLARD, L. 1980 *Int. J. Heat Mass Transfer* **23**, 1195.
VERONIS, G. 1963 *Astrophys. J.* **137**, 641.
WATSON, A. 1972 *Quart. J. Mech. Appl. Math.* **15**, 423.
WOODS, L. C. 1954 *Aero. Quart.* **5**, 176.